Charge Amplifier With an Enhanced Frequency Response for SPM-Based Data Storage

Hyunjoong Lee, *Student Member, IEEE*, Jong-Kwan Woo, *Student Member, IEEE*, Hyo-Jin Nam, Won-Hyeog Jin, Moongi Jeong, Young-Sik Kim, Jin-Koog Shin, and Suhwan Kim, *Senior Member, IEEE*

***Abstract*—Storage systems based on scanning probe microscopy incorporate an array of thermopiezoelectric cantilevers that require charge amplifiers with a wide frequency response but low power consumption. We use an improved frequency compensation method to enhance the in-band frequency response without requiring any additional power. Measurements show that the prototype chip draws the same 68 μA at 1.8 V as an unmodified design but has a closed-loop frequency response that is ten times greater. The chip was fabricated in a 0.18-μm standard CMOS process, and the charge amplifier core occupies 0.042 mm^2.**

***Index Terms*—Charge amplifier, CMOS, data storage, frequency compensation, lead zirconate titanate (PZT), microelectromechanical system (MEMS), scanning probe microscopy (SPM), thermopiezoelectric cantilever.**

I. INTRODUCTION

THE STORAGE density of conventional hard disk drives has continued to dramatically increase during recent decades. However, the well-known superparamagnetic effect will eventually limit the areal density of magnetic recording methods. Although some methods such as perpendicular recording are pushing at this limit, it is unlikely that densities beyond the order of 1 Tb/in^2 will easily be achieved.

Pioneering research [1], [2] has positioned scanning probe microscopy (SPM) as a promising alternative to overcome the density limit of magnetic storage [3]. Among the several SPM-based approaches, atomic force microscopy (AFM)-based storage is the most attractive since it offers the possibility of achieving a storage density of 1 Tbit/in^2 while also improving the data rates and the reliability of the writing operation [2], [3]. However, since the SPM technique is slow, we need parallel operation of multiple cantilevers to achieve a reasonable operational speed [2].

An AFM cantilever tip can perform read and write operations using either a thermomechanical mechanism [1], [2] or a thermopiezoelectric mechanism [4], [5]. In both cases, the writing mechanism is similar [2], [4], but the reading mechanism is different. In the thermomechanical mechanism, the tip is heated to measure the change in thermal conductance in terms of the thermal flow between the tip and the polymer substrate. Consequently, the readout circuitry may consume a lot of power in heating the tip [6]. However, in the thermopiezoelectric mechanism, a charge is self-generated without consuming power. Thus, the readout circuit only needs a charge amplifier to convert the charge into a voltage signal.

Recently [5], the route toward integrated high-density probe-based data storage has been pioneered, where a thermopiezoelectric cantilever array constructed as a microelectromechanical system (MEMS) was integrated with a CMOS circuit at the wafer level. To achieve this integration and to ensure the parallel operation of multiple cantilevers, a low-power high-density circuit design method is required. In addition, if we use the thermopiezoelectric mechanism, parallelization only increases the power requirements of the readout circuitry. In this case, the charge amplifier should have a wide bandwidth with low power consumption because charge amplifiers should work fast enough to meet the required speed of the data storage on a limited power budget. In this brief, we propose an improved frequency compensation method to achieve this goal. By implementing this method, the bandwidth of the main signal path can be extended, whereas the common-mode feedback (CMFB) signal path can separately be compensated to ensure phase margins.

II. THERMOPIEZOELECTRIC CANTILEVER

Fig. 1 is a diagram of a thermopiezoelectric cantilever fabricated as a MEMS [4]. As the cantilever tip encounters indentations while scanning over the polymer media, charges induced by the deflection of the cantilever are generated on the piezoelectric capacitor, which is composed of a lead zirconate titanate (PZT) film. This charge is generated by changes in strain in the sensor, and therefore, no external power supply is required. Fig. 2 shows a simplified circuit model of this piezoelectric sensor. The charge is not generated by the absolute strain but by the changes in strain as the dc component of the output signal is eventually removed by the resistance R_P. Hence, the value of R_P in the sensor is not a major concern, and

Manuscript received February 9, 2010; revised April 21, 2010; accepted May 11, 2010. Date of publication August 16, 2010; date of current version September 15, 2010. This work was supported in part by the Ministry of Knowledge Economy (MKE) of Korea through the program for the Development of the Next Generation Ultra-High Density Storage and in part by Pioneer R&D program for converging technology through the Korea Science and Engineering Foundation (KOSEF) funded by the Ministry of Education, Science and Technology under Grant M10711270001-08. This paper was recommended by Associate Editor P.-I. Mak.

H. Lee, J.-K. Woo, and S. Kim are with the Department of Electrical Engineering, Seoul National University, Seoul 151-742, Korea (e-mail: suhwan@snu.ac.kr).

H.-J. Nam, W.-H. Jin, and M. Jeong are with the Micro System Group, Devices and Materials Laboratory, LG Electronics Advanced Research Institute, Seoul 133-724, Korea.

Y.-S. Kim is with Zephyr Logic Inc., Seoul 135-841, Korea.

J.-K. Shin is with Korea Printed Electronics Center, Korea Electronics Technology Institute, Jeonju 561-844, Korea.

Color versions of one or more of the figures in this paper are available online at http://ieeexplore.ieee.org.

Digital Object Identifier 10.1109/TCSII.2010.2056030

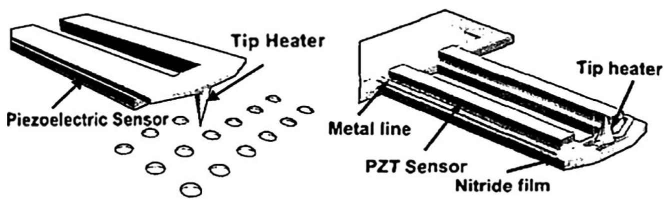

Fig. 1. Diagram of the thermopiezoelectric cantilever [4].

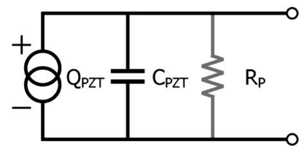

Fig. 2. Simplified circuit model of the piezoelectric sensor.

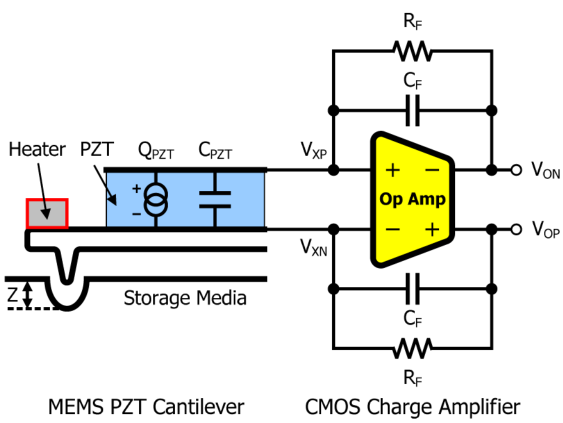

Fig. 3. Charge amplifier connected with the PZT cantilever.

there is no initial offset problem. As a result, the cantilever outputs the relative displacement only. This simplifies the model to be a charge source Q_{PZT} in parallel with a capacitance C_{PZT}. In this model, the charge is proportional to its sensitivity S_{PZT} and the vertical displacement Z of the cantilever tip. The relationship among them is shown in the following equation:

$$Q_{\mathrm{PZT}} = S_{\mathrm{PZT}} Z = C_{\mathrm{PZT}} V_{\mathrm{PZT}}. \tag{1}$$

V_{PZT} is the voltage generated if the piezoelectric sensor is seen as an equivalent voltage source. The characteristics of the PZT cantilever provided for the experiment are as follows: C_{PZT} is 100–250 pF, S_{PZT} is 0.615 fC/nm, and Z is 20–40 nm [4].

III. Charge Amplifier

A charge amplifier is required to convert the charges in the PZT cantilever into a voltage signal that can reliably be measured [7], [8]. Fig. 3 depicts the assembly of the charge amplifier with the PZT cantilever.

The operational amplifier (op amp) in the charge amplifier transfers the charge generated in the PZT cantilever to the feedback capacitor C_F. The charge stored in C_F is then amplified to output a voltage signal. The feedback resistor R_F controls the dc voltage at the input to the op amp, and it also determines the low-side cutoff frequency of the whole charge amplifier marked as $1/R_F C_F$ in the idealized frequency response of the charge amplifier, as depicted in Fig. 4. If we assume that the op amp has infinite gain, the ideal transfer characteristic that relates the input charge to the output voltage in the passband is given by

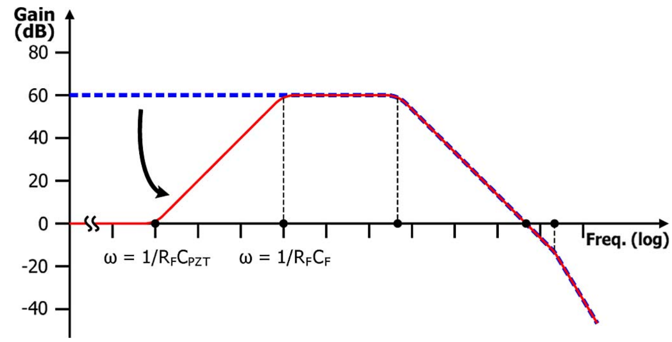

Fig. 4. Idealized frequency response of the charge amplifier.

$$V_O = -\frac{Q_{\mathrm{PZT}}}{C_F} = -\frac{S_{\mathrm{PZT}} Z}{C_F}. \tag{2}$$

To further reduce the environmental noise, the charge amplifier is implemented as a fully differential circuit. We adopted a two-stage differential folded-cascode op amp. In this configuration, the op amp requires a CMFB circuit with an error amplifier.

IV. Frequency Compensation

In a practical op amp, the open-loop gain and the gain–bandwidth product are not infinite. Both of them must be traded off against power consumption and circuit size [9]. Taking these factors into account, the transfer characteristic of the charge amplifier can be expressed as follows:

$$V_O = -\frac{Q_{\mathrm{PZT}}}{C_F\left(1+\frac{1}{A(f)}+\frac{C_{\mathrm{PZT}}}{A(f)\cdot C_F}\right)}. \tag{3}$$

If we assume that the open-loop gain of the op amp is very large, we can use the first-order approximation of this equation, i.e.,

$$V_O \simeq -\frac{Q_{\mathrm{PZT}}}{C_F}\left(1-\frac{C_{\mathrm{PZT}}}{A(f)C_F}\right). \tag{4}$$

The value of $A(f)$ must be sufficiently larger than the inverse of the feedback factor C_{PZT}/C_F. If C_{PZT} is 100 pF and C_F is 100 fF, $A(f)$ should be larger than 100 dB in the passband of the signal to maintain the gain error around 1%.

Fig. 5 shows a schematic of an op amp with the general frequency compensation, which has its dominant pole generated by a large Miller capacitor C at the output of the first stage and its nondominant pole at the output of the second stage. This kind of general-purpose frequency compensation creates adequate phase margins at the frequency at which the open-loop gain of the main signal path declines to 0 dB. This requires a large compensation capacitor but allows the op amp to operate with any configuration of feedback factor. The operation of this class of op amp can be better understood if it is visualized as separate transconductance and output impedance stages. Fig. 6 shows a block diagram of this form and the frequency response

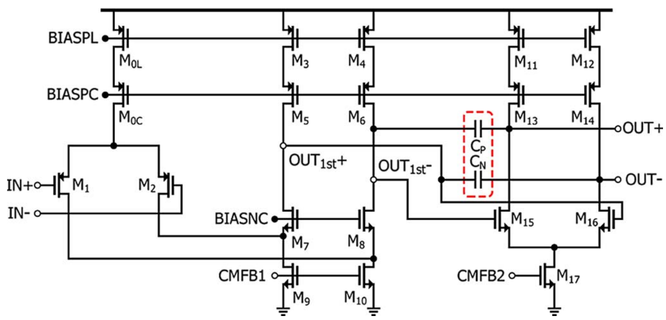

Fig. 5. Schematic of an op amp with general frequency compensation.

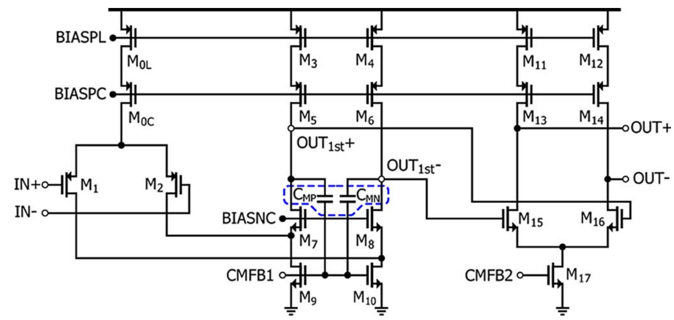

Fig. 8. Schematic of an op amp with enhanced frequency compensation.

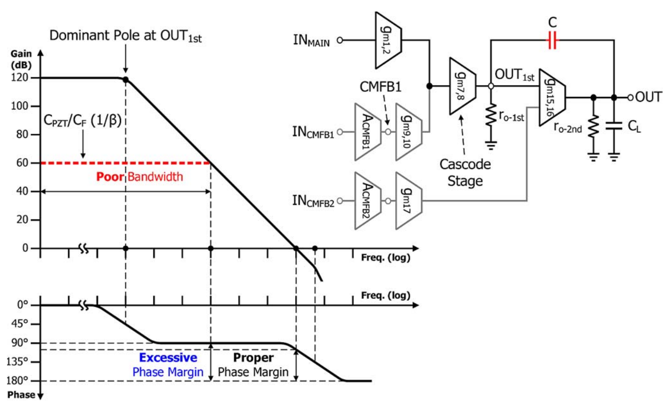

Fig. 6. Block diagram and frequency response of the main signal path with general frequency compensation (from $\mathrm{IN_{MAIN}}$ to OUT).

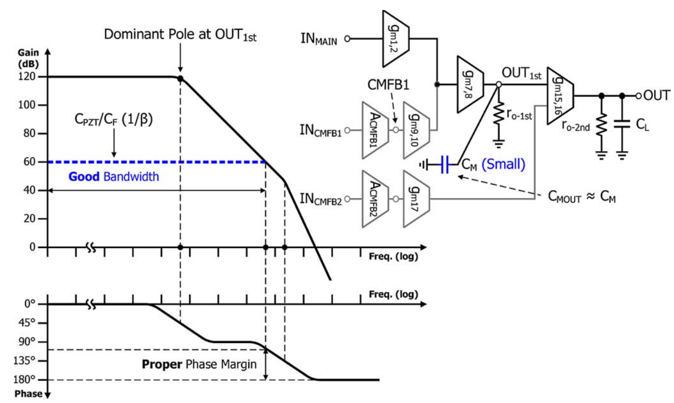

Fig. 9. Block diagram and frequency response of the main signal path with enhanced frequency compensation (from $\mathrm{IN_{MAIN}}$ to OUT).

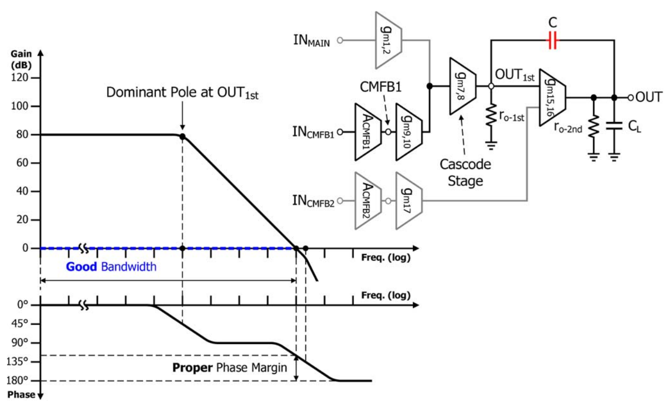

Fig. 7. Block diagram and frequency response of the CMFB signal path with general frequency compensation (from $\mathrm{IN_{CMFB1}}$ to $\mathrm{OUT_{1st}}$).

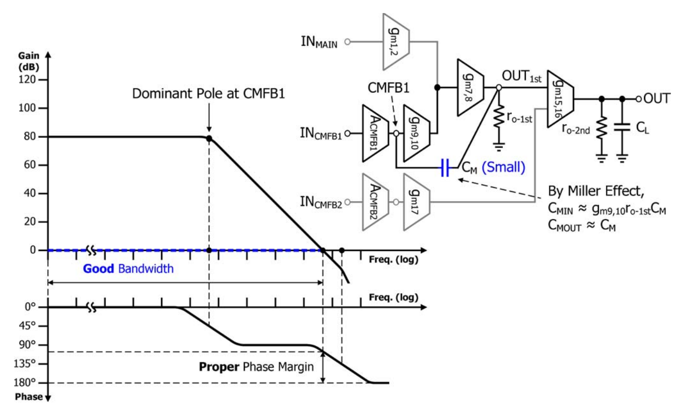

Fig. 10. Block diagram and frequency response of the CMFB signal path with enhanced frequency compensation (from $\mathrm{IN_{CMFB1}}$ to $\mathrm{OUT_{1st}}$).

of the main signal path. Fig. 7 shows the block diagram and the frequency response of the CMFB signal path. In the diagram, the error amplifier A_{CMFB1} senses the center level of the differential output and compares the level with a preferred common-mode voltage such as $V_{\mathrm{DD}}/2$. Then, the amplified error signal is fed back to the gate CMFB1 of $M_{9,10}$, as indicated in Fig. 5. We used all-CMOS CMFB error amplifiers for A_{CMFB1} and A_{CMFB2}, which have cross-coupled differential input pairs with diode-connected output loads and require no resistors for averaging the differential output to avoid resistive loading and to consume less circuit area.

For the compensation of the op amp, a Miller capacitor C is placed where the main path joins the CMFB path. The compensation that it provides stabilizes both paths simultaneously. In this case, if we want more bandwidth on the main path, more power will be required. Since an op amp designed for a PZT cantilever will only be used in a charge amplifier with high closed-loop gain, we can use an alternative approach. If the op amp is compensated at the point where the inverse of the feedback factor, such as 60 dB with 100 pF of C_{PZT} and 100 fF of C_F, crosses the frequency response of the main path, the bandwidth can be enhanced without any additional power consumption. Moreover, a smaller compensating capacitor requires less area. However, the CMFB path becomes unstable in this situation since it was originally compensated together with the main path by C and it still requires constant unity-gain compensation. Hence, the method that compensates the overall

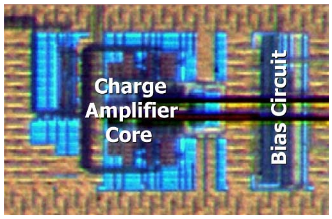

Fig. 11. Photograph of the charge amplifier chip.

TABLE I
CHARACTERISTICS OF THE CHARGE AMPLIFIER

Technology	0.18μm CMOS
Supply Voltage	1.8V
Open-loop DC Gain	125dB
Current Consumption	68μA
Core Area	0.042mm^2

negative feedback system for the main path cannot directly be applied to this fully differential circuit.

To solve this problem, a small capacitor C_M is added between the gate of the transistor $M_{9,10}$ and the output of the first stage while C is removed. Fig. 8 shows a schematic of an op amp with this form of enhanced frequency compensation method. Now, the frequency response of the main path is widened with a small value of C_M, which moves the dominant pole to a higher frequency, as shown in Fig. 9. However, this method effectively enlarges C_M for the CMFB path because of the Miller effect. The equivalent capacitance C_{MIN} seen from the gate of $M_{9,10}$ is approximately $g_{m9,10} r_{\text{o-1st}} C_M$, where $g_{m9,10}$ is the transconductance of $M_{9,10}$, and $r_{\text{o-1st}}$ is the equivalent output resistance seen from the output of the first stage. Hence, a small value of C_M effectively provides a large compensating capacitance for the CMFB path, and this path is stabilized, as depicted in Fig. 10. Consequently, the main path and the CMFB path can be suitably compensated independently. This method is also efficient in terms of power consumption and area.

V. Experimental Results

To assess the effectiveness of our enhanced frequency compensation method, a prototype chip was fabricated and measured in a 0.18-μm CMOS process with a 1.8-V power supply. Fig. 11 shows a photograph of the charge amplifier chip. The circuit core occupies 0.042 mm^2. The core of the charge amplifier consumes 68 μA with an open-loop dc gain of 125 dB. Table I summarizes the characteristics of the charge amplifier.

Figs. 12 and 13 show the simulated open- and closed-loop frequency responses of the charge amplifier before and after compensation. The value of C_{PZT} is 100 pF and that of C_F is 50 fF, to make the ideal closed-loop in-band gain 66 dB. Simulation results show that the closed-loop gain is almost matched above 64.5 dB. The enhanced frequency compensation widens the high-side cutoff frequency of the closed-loop response from 6.2 to 79.5 kHz.

Fig. 14 shows the measured closed-loop frequency response of the charge amplifier chip, when it is driven with a function generator that provides a signal that corresponds to the

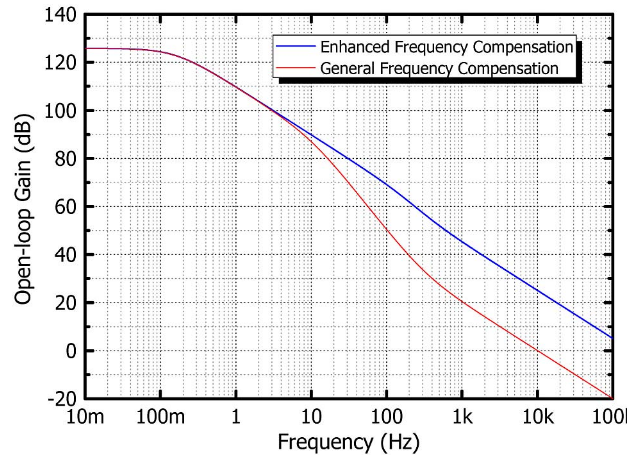

Fig. 12. Simulated open-loop frequency response of the charge amplifier.

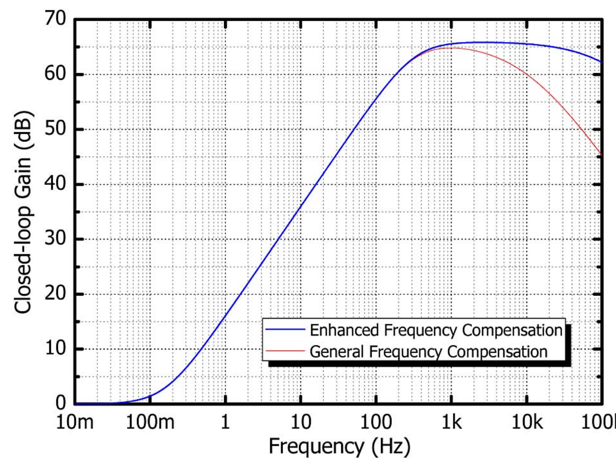

Fig. 13. Simulated closed-loop frequency response of the charge amplifier.

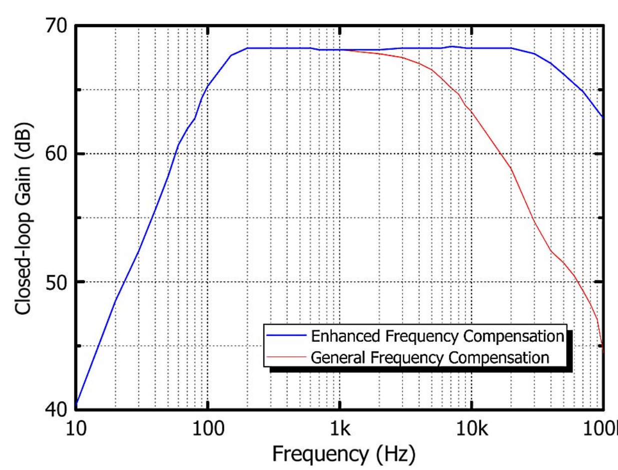

Fig. 14. Measured closed-loop frequency response of the charge amplifier.

voltage produced by the PZT cantilever, viewed as a voltage-equivalent circuit. C_{PZT} is set to 140 pF, and C_F is set to 50 fF. For testing purposes, R_F is set to 10 GΩ since the physical actuator for driving the PZT cantilever has to be driven with a low frequency such as 10 Hz. They correspond to 68 dB of the ideal closed-loop in-band gain. C_F is implemented as a metal–insulator–metal capacitor on the chip, whereas C_{PZT} and R_F are surface mounted on the test board. The in-band

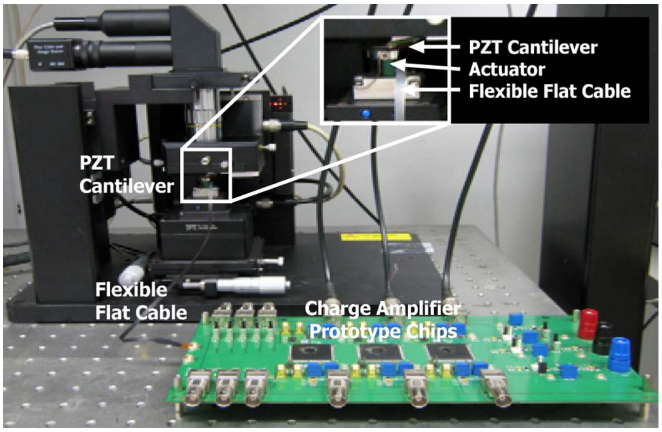

Fig. 15. Environment for testing with a PZT cantilever.

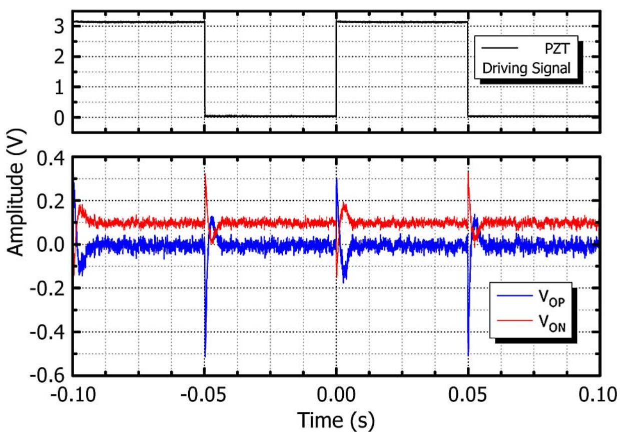

Fig. 16. Actuator driving signal and measured waveform of the charge amplifier output.

frequency response range of the charge amplifier over the gain of 65 dB is increased from 6.5 to 65 kHz by the proposed compensation method.

To assess the performance of the charge amplifier, it was directly connected to the output of a PZT cantilever with a flexible flat cable. The environment for testing is shown in Fig. 15. The cantilever was continuously driven by the actuator with a square signal at 10 Hz, which generated about 30 nm of vertical displacement of the cantilever tip. Fig. 16 shows the actuator driving signal and the measured waveform of the charge amplifier output. To reduce the effect of noise on the output, it was averaged on the oscilloscope. The peak-to-peak output voltage was about 840 mV. Assuming that the amplitude is 420 mV, and knowing that C_F is 50 fF, we can determine that the output charge is 21 fC. This corresponds to a sensitivity of 0.7 fC/nm, which shows a good match to the sensitivity of the provided cantilever for this experiment [4].

VI. Conclusion

The limited speed of SPM-based storage requires parallel operation of multiple AFM cantilevers. In this configuration, the thermopiezoelectric cantilevers require a charge amplifier with sufficient bandwidth and low power consumption. We used enhanced frequency compensation to extend the frequency response of a charge amplifier while limiting its power consumption. Measurements show that the method is effective and requires no additional power.

References

[1] P. Vettiger, M. Despont, U. Drechsler, U. Dürig, W. Häberle, M. I. Lutwyche, H. E. Rothuizen, R. Stutz, R. Widmer, and G. K. Binnig, "The "millipede"—More than one thousand tips for future AFM data storage," *IBM J. Res. Develop.*, vol. 44, no. 3, pp. 323–340, May 2000.

[2] E. Eleftheriou, T. Antonakopoulos, G. K. Binnig, G. Cherubini, M. Despont, A. Dholakia, U. Dürig, M. A. Lantz, H. Pozidis, H. E. Rothuizen, and P. Vettiger, "Millipede—A MEMS-based scanning-probe data-storage system," *IEEE Trans. Magn.*, vol. 39, no. 2, pp. 938–945, Mar. 2003.

[3] S. Hosaka, "SPM based recording toward ultrahigh density recording with trillion bits/inch^2," *IEEE Trans. Magn.*, vol. 37, no. 2, pp. 855–859, Mar. 2001.

[4] H.-J. Nam, Y.-S. Kim, C. S. Lee, W.-H. Jin, S. Jang, I.-J. Cho, and J.-U. Bu, "Integrated nitride cantilever array with Si heaters and piezoelectric detectors for nano-data-storage application," in *Proc. 18th IEEE Int. Conf. MEMS*, 2005, pp. 247–250.

[5] Y.-S. Kim, H.-J. Nam, S. Jang, C. S. Lee, W.-H. Jin, I.-J. Cho, J.-U. Bu, S.-I. Chang, and E. Yoon, "Wafer-level transfer of thermo-piezoelectric Si_3N_4 cantilever array on a CMOS circuit for high density probe-based data storage," in *Proc. 19th IEEE Int. Conf. MEMS*, Istanbul, Turkey, 2006, pp. 922–925.

[6] C. Hagleitner, T. Bonaccio, H. Rothuizen, D. Wiesmann, J. Lienemann, J. Korvink, G. Cherubini, and E. Eleftheriou, "Modeling, design, and verification for the analog front-end of a MEMS-based parallel scanning-probe storage device," in *Proc. IEEE CICC*, 2006, pp. 193–196.

[7] W. J. Marbie, K. Kotani, and C. S. Petrie, "Practical charge-transfer amplifier design architectures for low-power Flash A/D converters," *IEEE Trans. Circuits Syst. I, Reg. Papers*, vol. 51, no. 11, pp. 2157–2164, Nov. 2004.

[8] S.-Y. Peng, M. S. Qureshi, P. E. Hasler, A. Basu, and F. L. Degertekin, "A charge-based low-power high-SNR capacitive sensing interface circuit," *IEEE Trans. Circuits Syst. I, Reg. Papers*, vol. 55, no. 7, pp. 1863–1872, Aug. 2008.

[9] A. E. Mourabit, G.-N. Lu, and P. Pittet, "Wide-linear-range subthreshold OTA for low-power, low-voltage, and low-frequency applications," *IEEE Trans. Circuits Syst. I, Reg. Papers*, vol. 52, no. 8, pp. 1481–1488, Aug. 2005.